Structural and Optical Properties of Burr-Like CuS/Cu_9S_5 Microwires and Cu_9S_5 Microspheres Synthesized by a Two-Step Solvothermal Method

Libo Fan,*[1,2] Tuanhui Feng,[1] Peng Wang,[1] Chunli Zhang,[1] and Zhibo Feng[1]

[1]College of Electrical and Information Engineering, Xuchang University, 88 Ba-Yi Road, Xuchang 461000, P. R. China

[2]Institute of Surface Micro and Nano Materials, Xuchang University, 88 Ba-Yi Road, Xuchang 461000, P. R. China

Received February 6, 2009; E-mail: fanlibo_2004@yahoo.com.cn

Burr-like CuS/Cu_9S_5 microwires and Cu_9S_5 microspheres can be synthesized by a two-step solvothermal method. Experiment results indicated that the CuS/Cu_9S_5 microwires (diameter of ca. 300 nm and length of several micrometers) and Cu_9S_5 microspheres (diameter of ca. 800 nm) obtained by this method had uniform morphologies and large product. X-ray diffraction (XRD), high-resolution transmission electron microscopy (HR-TEM), and field-emission scanning electron microscopy (FE-SEM) experiments were carried out to characterize them. Fourier transform infrared (FT-IR) spectra and thermogravimetric analysis (TGA) experiments were carried out to study the components and thermal stabilization of the precursors. A possible formation mechanism and ultraviolet–visible (UV–vis) absorption spectra are also described in this paper.

Copper sulfides have drawn significant interest due to their variations in stoichiometric composition, valence states, morphologies, structures, and properties.[1–5] The stoichiometric composition of copper sulfide varies in a wide range from Cu_2S at the copper-rich side to CuS_2 at the copper-deficient side. For example chalcocite (Cu_2S), djuleite ($Cu_{1.96}S$), digenite ($Cu_{1.8}S$), and covellite (CuS) are several known solid phases at room temperature.[6,7] Copper sulfides have lots of potential applications in numerous fields, such as photothermal conversion, p-type semiconductors in solar cell devices, switches, coatings for microwave shields in the form of thin films, super ionic materials, optical filters, and room temperature ammonia gas sensors.[8–12]

Up to now, different techniques have been used to prepare nanocrystals, such as electrodeposition, vapor transport, vapor deposition, vapor–liquid–solid processs, and solvothermal methods.[1,2,6,13–17] Some methods have inevitable limitations, such as complex processing steps, the use of toxic hydrogen sulfide gas and the need of high temperature, expensive reactants or reactors. However, the solvothermal method has some advantages, such as simplicity, low cost, low operating temperature, environmental friendliness, and high reproducibility by control over shape/size and desired stoichiometry.

In this paper, burr-like CuS/Cu_9S_5 microwires and Cu_9S_5 microspheres can be synthesized by a two-step solvothermal method. First, burr-like CuS/pyridine hybrid microwires and microspheres were synthesized as precursors. After extracting the precursors, burr-like CuS/Cu_9S_5 microwires and Cu_9S_5 microspheres were obtained. A possible growth mechanism is given based on a series of experiments. Characterizations and optical absorption experiments were also carried out.

Experimental

Sample Preparation. Cupric acetate ($Cu(CH_3COO)_2\cdot H_2O$), thiourea ($(NH_2)_2CS$), pyridine (C_5H_5N), and ethylene glycol ($HOCH_2CH_2OH$) were analytical grade reagents and were all used as received without further purification.

In a typical synthesis, 2.4 mL of 0.25 M $Cu(CH_3COO)_2\cdot H_2O$ and 2.4 mL of 0.5 M $(NH_2)_2CS$ aqueous solution were added to 60 mL of C_5H_5N at room temperature under magnetic stirring and the volume ratio of water to pyridine (V_{water}:$V_{pyridine}$) was 1:12.5. After stirring for 30 min, the resultant solution was transferred into two 50-mL Teflon line stainless steel autoclaves (TSSAs) and then maintained in an oven at 100 °C for 20 h. After the reaction, the TSSAs were cooled naturally to room temperature. To remove reactants possibly remaining in the final product, the product was washed with ethanol several times by centrifuge. The black precipitates collected from one TSSA were dried at 80 °C for 10 h under vacuum. Finally, sample **A** (CuS/pyridine microspheres) was obtained.

To extract, a sample collected from another TSSA was redispersed in 30 mL of ethylene glycol under magnetic stirring for 30 min. A suspension formed and was transferred into a 50-mL TSSA. The TSSA was then kept in an oven at 180 °C for 48 h. The gray product was cooled, washed, centrifuged, and dried just like sample **A**, and was then labeled sample **B** (Cu_9S_5 microspheres).

The synthetic process of sample **C** (CuS/pyridine microwires) was the same as that of sample **A**, but the solvent was a mixture of 6 mL of pyridine and 54 mL of deionized water instead of 60 mL of pure pyridine. Note that the total volume of water was 58.8 mL, which included 54 mL of pure deionized water, 2.4 mL of 0.25 M $Cu(CH_3COO)_2\cdot H_2O$, and 2.4 mL of 0.5 M $(NH_2)_2CS$ aqueous solution. So the ratio of V_{water}:$V_{pyridine}$ for the preparation of sample **C** was 10:1, approximately. The color of sample **C** was black. The synthetic process for sample **D** (CuS/Cu_9S_5 microwires) was the same as that for sample **B**, except for using

Published on the web August 7, 2009; doi:10.1246/bcsj.82.1015

Table 1. Reaction Conditions of Different Samples

Reaction conditions	Samples									
	A	**B**	**C**	**D**	**E**	**F**	**G**	**H**	**I**	**J**
Solvent V_{water}:$V_{pyridine}$	1:12.5	1:12.5	10:1	10:1	1:12.5	1:12.5	1:12.5	1:12.5	no water	no pyridine
Reactant quantity/mmol										
$Cu(CH_3COO)_2 \cdot H_2O$	0.6	0.6	0.6	0.6	0.15	0.3	1.2	2.4	0.6	0.6
$(NH_2)_2CS$	1.2	1.2	1.2	1.2	0.3	0.6	2.4	4.8	1.2	1.2
Extraction using ethylene glycol	No	Yes	No	Yes	No	No	No	No	No	No

sample **C** as the precursor instead of sample **A**. The color of sample **D** was between gray and black.

The synthetic processes for samples **E**, **F**, **G**, and **H** were the same as that of sample **A**, except the concentrations of $Cu(CH_3COO)_2 \cdot H_2O$ and $(NH_2)_2CS$ used in the preparation were 25%, 50%, 2 and 4 times of those used in sample **A**, respectively.

Sample **I** was obtained by adding 119.8 mg of $Cu(CH_3COO)_2 \cdot H_2O$ and 91.3 mg of $(NH_2)_2CS$ to 64.8 mL of pyridine with no added water. Sample **J** was obtained by using 60 mL of deionized water as solvent instead of 60 mL of pyridine. Note that the total volume of the solvent here was 64.8 mL, which included 60 mL of pure deionized water, 2.4 mL of 0.25 M $Cu(CH_3COO)_2 \cdot H_2O$, and 2.4 mL of 0.5 M $(NH_2)_2CS$ aqueous solution with no pyridine. The synthetic processes of samples **I** and **J** were also the same as that of sample **A**. For comparison, the reaction conditions of all samples are listed in Table 1.

Measurements. The X-ray diffraction (XRD) patterns were obtained on a Rigaku D/Max 2500V PC diffractometer operated at 18 kW with Cu Kα radiation ($\lambda = 1.5406$ Å). The transmission electron microscopy (TEM) images, high-resolution transmission electron microscopy (HR-TEM) images, and the fast Fourier transform (FFT) images of the HR-TEM images were recorded on a JEM-3010 transmission electron microscope under a working voltage of 300 kV. The field-emission scan electron microscopy (FE-SEM) images were measured on a Hitachi S4800 field emission scanning electron microscope. The Fourier transform infrared (FT-IR) spectra were recorded on a FTS-3000 Bio-Rad spectrophotometer. The thermogravimetric analysis (TGA) was conducted on a Perkin-Elmer Pyris Diamond thermogravimetric analyzer under nitrogen atmosphere (with a heating rate of 10 °C min^{-1}, 40–400 °C). The ultraviolet–visible (UV–vis) absorption spectra were measured on an UV-3101PC UV-VIS-NIR scanning spectrophotometer (SHIMADZU). The powder samples used here were re-dispersed in ethanol by ultrasound to form a uniform suspension.

Results and Discussion

Characterizations. XRD Patterns: The XRD patterns of samples **A**–**D** in contrast to standard JCPDS cards of CuS (covellite, No. 76-1725) and Cu_9S_5 (digenite, No. 47-1748) are shown in Figure 1 of curves a)–f), respectively. Sample **A** is a composite of CuS and pyridine. Comparing the curves Figure 1a with Figure 1e, the broad peaks at 27.4, 29.2, 31.8, 48.0, and 58.8° can be correlated to covellite CuS, which are diffraction overlaps of several planes. For example, the peak at 29.2° corresponds to (100), (101), and (102) planes. Broadening of diffraction peaks is indicative of small crystallite sizes of CuS. The remaining peaks are relative strong and sharp

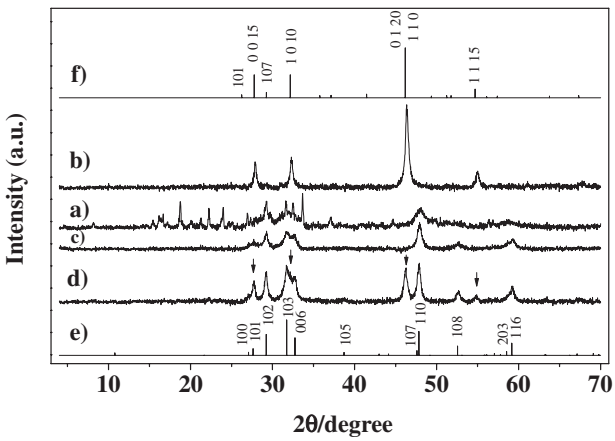

Figure 1. XRD patterns of various samples. a) Sample **A** (CuS/pyridine microspheres), b) sample **B** (pure Cu_9S_5 microspheres), c) sample **C** (CuS/pyridine microwires), d) sample **D** (CuS/Cu_9S_5 microwires), and the standard JCPDS cards of e) CuS (covellite, No. 76-1725) and f) Cu_9S_5 (digenite, No. 47-1748). The diffraction peaks of Cu_9S_5 are marked with arrows in d).

and cannot be indexed to any JCPDS cards of copper sulfide, which should come from the crystallization of pyridine in the sample **A**. Similar results was also observed in other inorganic–organic composites.[13,14] After extracting, the pyridine in sample **A** was completely removed, and CuS was changed into Cu_9S_5 in sample **B** (Figure 1b). The reaction mechanism will be discussed below. Sample **C** is also an inorganic–organic composite of CuS and pyridine, however it exhibits the diffraction peaks of CuS only (Figure 1c). According to the following HR-TEM and TGA results, it can be concluded that the quantity of pyridine in sample **C** is much less than that in sample **A**. So it is comprehensible that the diffraction peaks of pyridine are not seen in sample **C**. In Figure 1d, the diffraction peaks originating from CuS and Cu_9S_5 can both be seen. Sample **D** is a composite of CuS and Cu_9S_5, which can be supported by the following HR-TEM results and discussions on the reaction mechanisms in section: The Reaction Mechanism in Extraction.

FE-SEM and TEM Images: The microstructure study of samples **A**–**D** was conducted by FE-SEM and TEM experiments. Figure 2 shows the FE-SEM images of the samples **A** (CuS/pyridine composite) and **B** (pure Cu_9S_5). As shown in Figures 2a and 2b, samples **A** and **B** are uniform microspheres

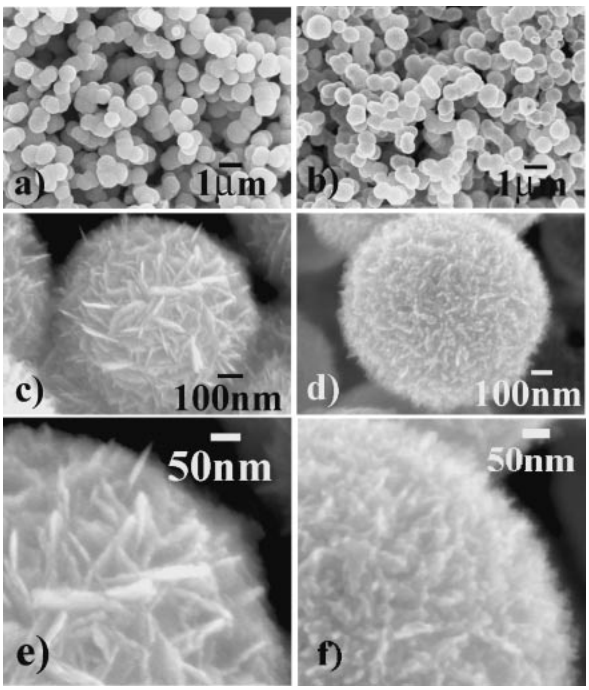

Figure 2. FE-SEM images of samples **A** and **B**. a) Sample **A** (CuS/pyridine microspheres), b) sample **B** (pure Cu_9S_5 microspheres), c) and e) the magnified images of sample **A**, and d) and f) the magnified images of sample **B**.

with average diameter of ca. 800 nm. As shown in Figures 2c and 2e, the magnified images of the Figure 2a, there are a great deal of flakes on the microsphere (burr-like) and their thickness is about 10–20 nm. As shown in Figures 2d and 2f, the enlarged images of Figure 2b, sample **B** has similar structures, however, the flakes became irregular and are smaller than those in sample **A**. Figure 3 shows the TEM images of the samples **A** and **B**. As shown, the microspheres in sample **A** are solid and black (Figures 3a and 3c), while the microspheres in sample **B** are brighter and seemed to be semitransparent (Figures 3b and 3d). A large number of pin holes formed in sample **B** due to the disappearance of pyridine in it by extracting sample **A** (Figures 3d and 3f). In the magnified images, the flakes can be also seen on the fringes of the microspheres (Figures 3e and 3f).

Figure 4 and Figure 5 show the FE-SEM and TEM images of samples **C** (CuS/pyridine composite) and **D** (CuS/Cu_9S_5 composite), respectively. As shown in Figures 4a and 4b, samples **C** and **D** both yield uniform microwires ca. 300 nm in diameter and several micrometers in length. As shown in Figure 4c, the magnified image of Figure 4a, the microwire in sample **C** has flake-like structures with flake thickness of 10–20 nm. As seen in Figure 4d, sample **D** has similar structures. The TEM images of Figures 5a and 5b indicate that the microwires in samples **C** and **D** are nearly the same. The color of the microwires in sample **D** (Figure 5d) is a little bit lighter than that in sample **C** (Figure 5c), however, it is not as semitransparent as the microspheres in sample **B** (Figures 3b, 3d, and 3f). That implies that pyridine disappeared in sample **D** and the quantity of pyridine in sample **C** is less than that in sample **A**, which can be also confirmed by other characterization methods.

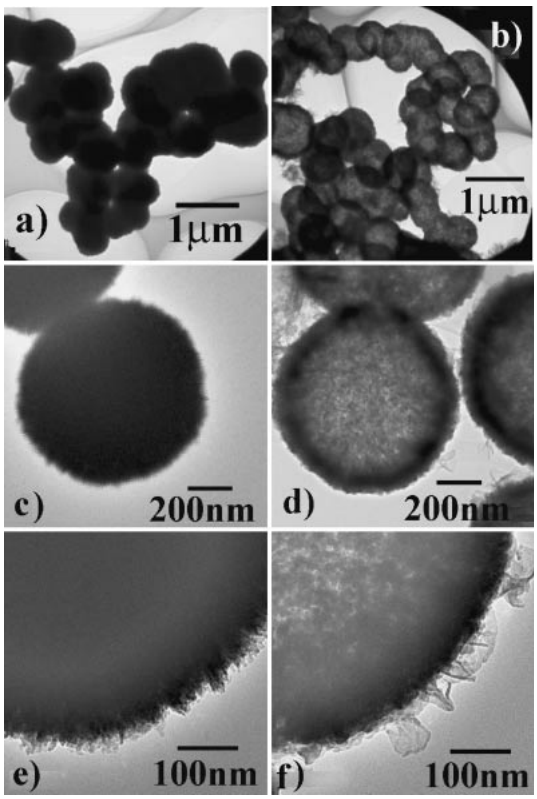

Figure 3. TEM images of samples **A** and **B**. a) Sample **A** (CuS/pyridine microspheres), b) sample **B** (pure Cu_9S_5 microspheres), c) and e) the magnified images of sample **A**, and d) and f) the magnified images of sample **B**.

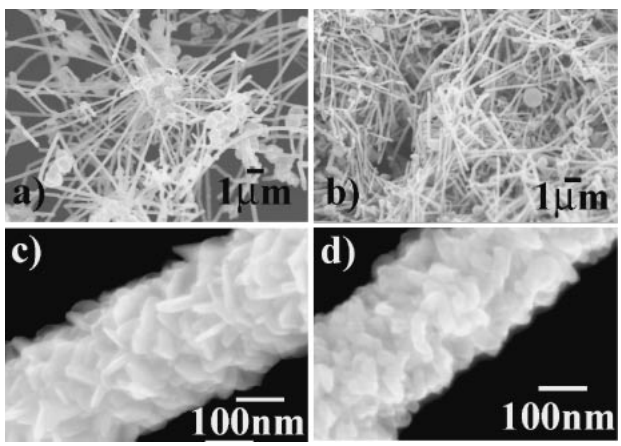

Figure 4. FE-SEM images of samples **C** and **D**. a) Sample **C** (CuS/pyridine microwires), b) sample **D** (CuS/Cu_9S_5 microwires), c) the magnified image of a), and d) the magnified image of b).

HR-TEM Patterns: The HR-TEM patterns of samples **A**–**D** and their corresponding FFT images are shown in Figure 6 and Figure 7, respectively. As shown in Figure 6a, crystalline zones and amorphous zones are interlaced in sample **A** (CuS/pyridine microspheres), which formed sub-nanostructures. In the crystalline zones, the interplanar distance is calculated to be 3.2083 Å, which coordinates with the distance of (101) planes of CuS. The width of the crystalline zones is smaller than 5 nm. The amorphous zones might come from the pyridine in the

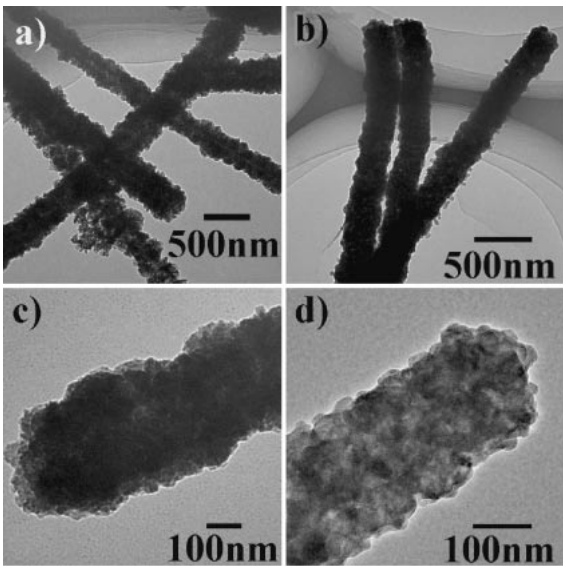

Figure 5. TEM images of samples **C** and **D**. a) Sample **C** (CuS/pyridine microwires), b) sample **D** (CuS/Cu_9S_5 microwires), c) the magnified image of a), and d) the magnified image of b).

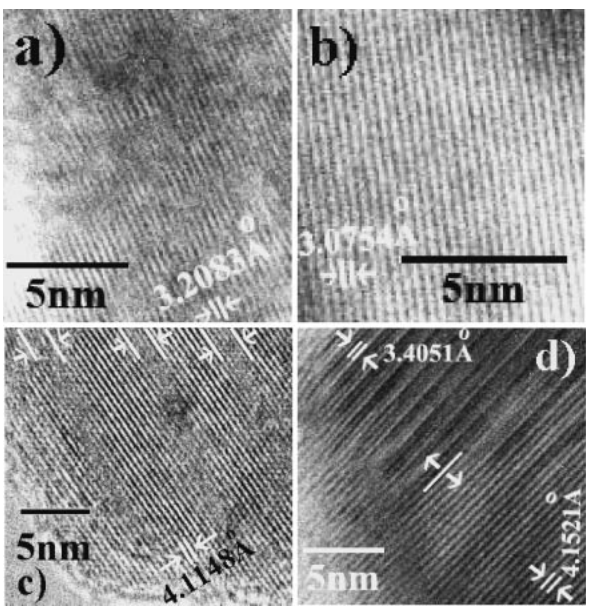

Figure 6. HR-TEM images of various samples. a) Sample **A** (CuS/pyridine microspheres), b) sample **B** (pure Cu_9S_5 microspheres), c) sample **C** (CuS/pyridine microwires), and d) sample **D** (CuS/Cu_9S_5 microwires).

composite, which make the whole composite demonstrates polycrystalline structure, thus a polycrystalline ring can be seen in Figure 7a. As shown in Figure 6b, a perfect crystal lattice can be seen in a relative big crystalline zone in sample **B** (Cu_9S_5 microspheres), the interplanar distance is calculated to be 3.0754 Å, which corresponds to the distance of (107) planes of Cu_9S_5. The diffraction dots coming from one single-crystalline plane can be observed in Figure 7b. Note that the synthetic temperature of sample **A** was 100 °C but the extraction temperature was 180 °C, so it is reasonable that the extraction product can restructure its crystal lattice at such a

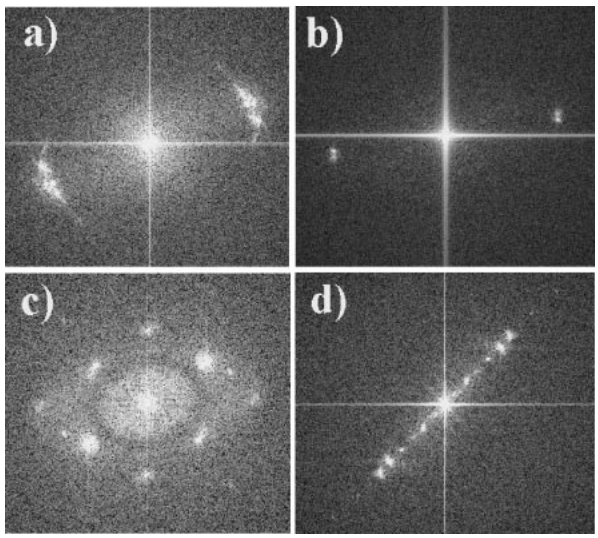

Figure 7. FFT images: a), b), c), and d) correspond to Figures 6a, 6b, 6c, and 6d, respectively.

high temperature to form sample **B**. After extracting the pyridine out of sample **A**, some gaps formed surround the crystalline zones of Cu_9S_5 in sample **B** (Figures 3d and 3f). These gaps still separated one nano-flake into different sub-regions. The width of one crystalline region reaches to ca. 5 nm.

In Figure 6c, crystalline bands are separated by amorphous bands, which are marked in the figure. The thickness of the crystalline bands is about 4 nm. The interplanar distance is calculated to be 4.1184 Å, which corresponds to the distance of (004) planes of CuS. The amorphous bands should also come from the pyridine in the composite of sample **C** (CuS/pyridine microwires). A hexagonal structure can be seen in Figure 7c. In Figure 6d, two crystal lattices of CuS and Cu_9S_5 can be seen in sample **D** (CuS/Cu_9S_5 microwires), which are distinguished along the diagonal of the figure. Above the diagonal, the interplanar distance is calculated to be 3.4051 Å, which corresponds to the distance of (101) planes of Cu_9S_5. Behind the diagonal, the interplanar distance is calculated to be 4.1521 Å, which corresponds to the distance of (004) planes of CuS. The HR-TEM patterns further indicate that sample **D** is a composite of CuS and Cu_9S_5. Diffraction dots coming from two or more planes can be seen in Figure 7d.

TGA Results: To determine the thermal stabilization of CuS/pyridine composites and the relative content of pyridine in them, TGA experiments were carried out and the results are shown in Figure 8. According to Figure 8a, one-step weight loss can be seen in sample **C** (CuS/pyridine microwires). The composite was stable below 230 °C and lost pyridine gradually over this temperature. The weight loss completed at about 350 °C. The net weight loss was 8.2%. In Figure 8b, three-step weight loss can be seen in sample **A** (CuS/pyridine microspheres). The first (68–87 °C), the second (190–210 °C), and the third (240–320 °C) steps had the net weight losses of 3.4%, 4.5%, and 16.6%, respectively.

According to the XRD results (Figure 1), the XRD peaks of the crystallized pyridine (the sharp ones) can be seen in sample **A**, however they were not been seen in sample **C**. The existence of pyridine in samples **A** and **C** can also be seen by

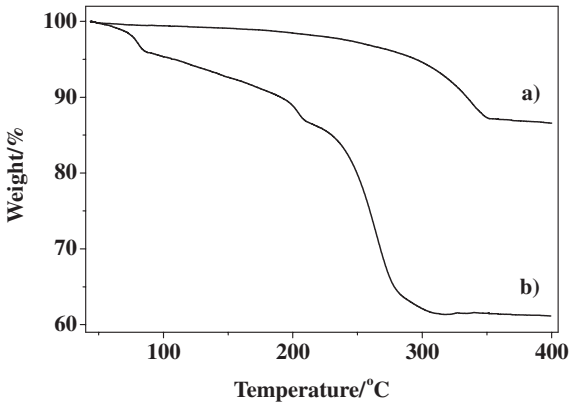

Figure 8. TGA curves: a) sample **C** (CuS/pyridine microwires) and b) sample **A** (CuS/pyridine microspheres).

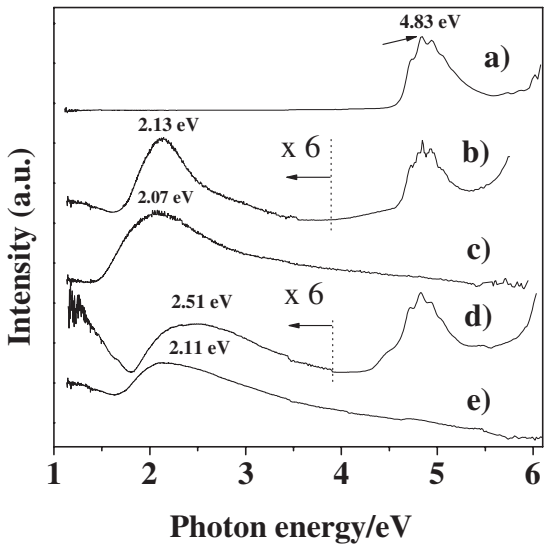

Figure 9. Absorption spectra: a), b), c), d), and e) corresponding to pure pyridine solution, samples **A** (CuS/pyridine microspheres), **B** (pure Cu_9S_5 microspheres), **C** (CuS/pyridine microwires), and **D** (CuS/Cu_9S_5 microwires), respectively. To show clearly, the intensity of the low energy sides (lower than 3.90 eV) of the curves b) and d) are magnified by 6 times.

the TEM, FT-IR experiments above, and the UV–vis absorption spectra below. Therefore, pyridine should consist of two parts in sample **A**, one free and one crystallized. There is only free pyridine in sample **C**. One-step weight loss seen in sample **C** should come from the loss of free pyridine. Comparing with sample **C**, the weight loss at the first and the second steps might come from the loss of the crystallized pyridine and the weight loss at the third step could be caused by the loss of free pyridine from sample **A**. Nevertheless, the quantity of pyridine in sample **A** is more than that in sample **C**.

UV–Vis Absorption Spectra. Figure 9 shows the UV–vis absorption spectra of samples **A**–**D**. As seen in Figure 9a, a broad absorption band centered at 4.8 eV can be observed in pyridine, which can be further resolved into four peaks, located at 4.72, 4.83, 4.94, and 5.04 eV, respectively. The same absorption band originating from pyridine can be also observed in Figures 9b and 9d, indicating the existence of pyridine in both samples **A** (CuS/pyridine microspheres) and **C** (CuS/pyridine microwires). Besides, another broad band around 2.13 eV appears in sample **A** (Figure 9b), while a band around 2.51 eV appears in sample **C** (Figure 9d), which are both attributed to the band gap absorptions of CuS. As shown in Figures 9c and 9e, the absorption peaks caused by the pyridine disappeared because the pyridine was extracted completely out of samples **B** (Cu_9S_5 microspheres) and **D** (CuS/Cu_9S_5 microwires). Furthermore, the band gap absorption of Cu_9S_5 around 2.07 eV appears in sample **B** (Figure 9c) and the band gap absorption of CuS/Cu_9S_5 around 2.11 eV appears in sample **D** (Figure 9e). It is well known, bulk Cu_2S (chalcocite) has a characteristic absorption edge at 1022 nm (ca. 1.21 eV), bulk CuS (covellite) has a characteristic broad absorption band at 920 nm (ca. 1.35 eV) and the absorption bands of copper sulfides shift blue with decreasing copper content.[18–24] So the characteristic absorption energy of bulk Cu_9S_5 (digenite) should be between 1.21 and 1.35 eV. Comparing with the characteristic absorption positions of their corresponding bulk materials, all band gap absorptions of samples **A**–**D** blue shift, which can be attributed to quantum confinement effect (QCE), however, the diameter of the CuS/pyridine and Cu_9S_5 spheres (samples **A** and **B**) or the CuS/pyridine and CuS/Cu_9S_5 wires (samples **C** and **D**) are bigger than nanometer range. What is the reason? The spheres and the wires are composed of large numbers of nanoflakes (Figures 2–5) and the nanoflakes have sub-nanostructures (Figure 6). The size of the crystalline zone of copper sulfide in the sub-nanostructures are all smaller than 5 nm in samples **A**–**D**, which have been illustrated in their HR-TEM patterns above, so the restriction of size and size distribution are exhibited in the sub-nanostructures instead of the actual dimensions and the size of samples **A**–**D**. The occurence of QCE should be related to the size confinement of the nanoflakes in the thickness direction and the existent of sub-nanostructures in flakes. Note that the sub-nanostructures did not disappear completely even after extraction (samples **B** and **D**), because gaps formed instead in the locations of pyridine, which can also be identified by the TEM and HR-TEM images above.

The Possible Formation Mechanism. The Growth Mechanism: To suggest a possible growth mechanism, many experiments on sample preparation were carried out, changing the reaction conditions, such as temperature, time, the reactant concentrations, and the ratios of V_{water}:$V_{pyridine}$ in the solvent. The results indicate burr-like CuS/pyridine microspheres can be synthesized from 80 to 200 °C and from 2 h to 10 days. High temperature and long reaction time can improve the crystallinity of the microspheres. By varying the reactant concentrations, the diameters of the spheres can be changed from 300 nm to 2 μm, samples **E**–**H** as shown in Figures 10a–10d. Low reactant concentration produced small spheres and high reactant concentration produced large ones. When no water was added and only pyridine served as solvent, burr-like CuS/pyridine microspheres could also be obtained, however their size distribution was inhomogeneous (sample **I** as shown in Figure 10e. When the ratio of V_{water}:$V_{pyridine}$ came to be 1:12.5 (sample **A**), microspheres with homogeneous size distribution were obtained. Further increasing the quantity of water in the solvent, burr-like CuS/pyridine microwires appeared. When

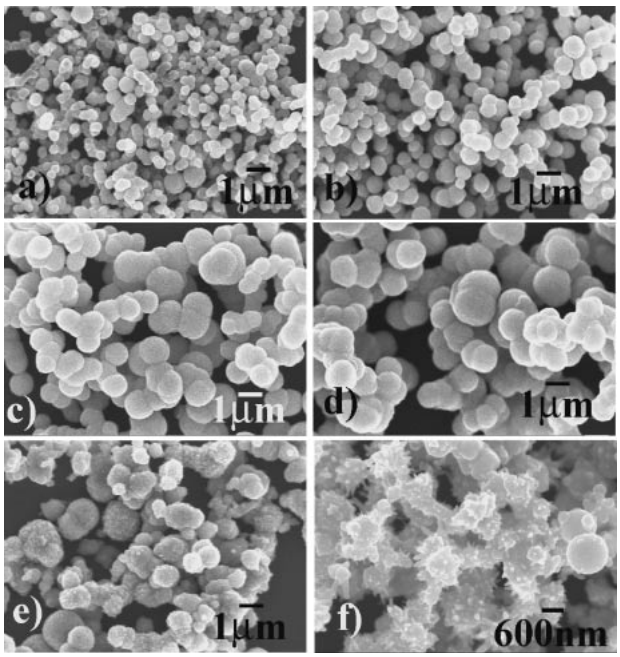

Figure 10. FE-SEM images: a), b), c), d), e), and f) correspond to the whole morphologies of samples **E**, **F**, **G**, **H**, **I**, and **J**, respectively.

the ratio of V_{water}:$V_{pyridine}$ came to be 10:1 (sample **C**), homogeneous microwires were obtained. Further increasing the quantity of water in the solvent, the quantity of microwires decreased and particles appeared. When no pyridine was added and only water served as solvent, pure CuS particles with irregular morphologies and sizes were obtained (sample **J**, see Figure 10f). In a word, the reactant concentrations can determine the sizes of CuS/pyridine composites and the ratios of V_{water}:$V_{pyridine}$ can play a key role in controlling the morphologies of the composites.

On the basis of the above experiment results, a growth mechanism of CuS/pyridine composites could be proposed, which is crucial to control the whole chemical reaction. In fact, after water is added to pyridine, we can simply consider that a quasi-emulsion system formed, in which the amount of water plays a key role. When a little water was added to pyridine, water was dispersed into a great number of small drops after stirring and surrounded by pyridine. We call them spherical micelles (Figure 11c and step **I** on the left-hand side of Figure 11). Increasing the quantity of water to another suitable value, uniform and regular wire-like micelles formed (see Figure 11d and step **I** on the right-hand side of Figure 11). While without water and only pyridine serving as solvent, a quasi-emulsion system could not form. When excess water was added, it existed as continuous phase of water and pyridine and the quasi-emulsion system could not form either.

The reactants were contained in water (cupric acetate and thiourea in this work) and coordinate bonds formed between >N of pyridine and Cu^{2+} inside the reverse micelles, so micelles served as microreaction containers (Figures 11a and 11b). In certain solvothermal conditions (above 80 °C), S^{2-} was released from thiourea. In this case, CuS species formed subsequently inside the spherical micelles and grew

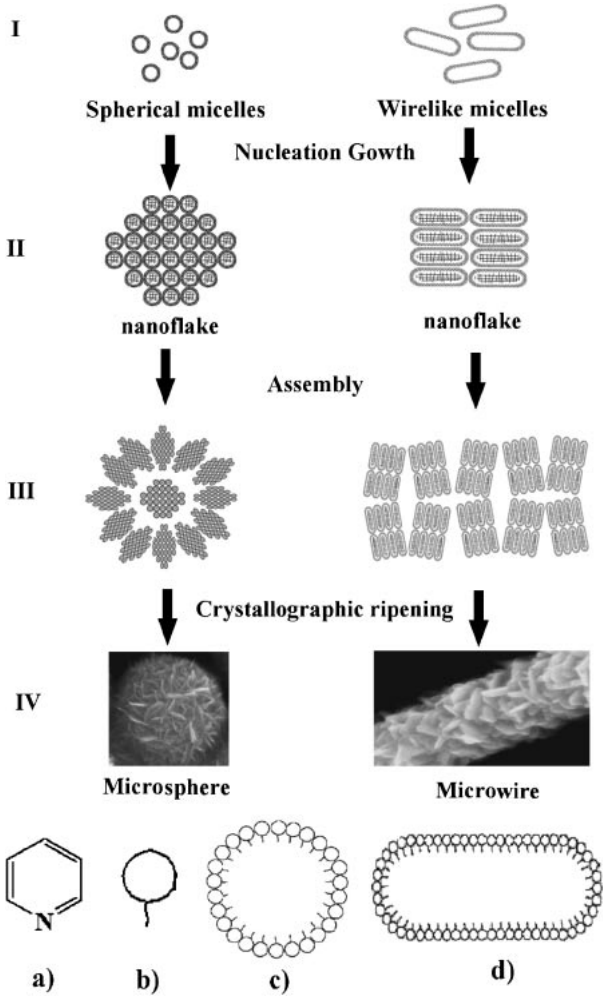

Figure 11. Schematic illustrations of a possible growth mechanism of burr-like CuS/pyridine microspheres on the left-hand side and burr-like CuS/pyridine microwires on the right-hand side. a) The structure scheme of one pyridine molecule, the schematic images: b) one pyridine molecule, c) one of the spherical micelles as shown on the left-hand side of step **I**, and d) one of the wire-like micelles as shown on the right-hand side of step **I**.

into wafer-like or rectangular nanoflakes (see step **II** of Figure 11). Through self-assembly, nanoflake-based microspheres or microwires formed (see step **III** of Figure 11). After crystallographic ripening, burr-like CuS/pyridine microspheres or microwires were finally obtained (see step **IV** of Figure 11).

The Reaction Mechanism in Extraction: By extracting the pyridine out of the precursors, the basic morphologies of the precursors did not change and CuS/Cu_9S_5 microwires and Cu_9S_5 microspheres were obtained. Redox reactions occurred after extraction. The CuS/pyridine microspheres (sample **A**) changed to pure Cu_9S_5 microspheres (sample **B**) and the CuS/pyridine microwires (sample **C**) changed to CuS/Cu_9S_5 microwires (sample **D**), which are supported by the XRD and HR-TEM results. The redox reactions could be caused by either ethylene glycol (the extraction solution) or CuS itself. In order to reveal this point, the FT-IR spectra of ethylene glycol solutions, before and after extracting, and pure pyridine

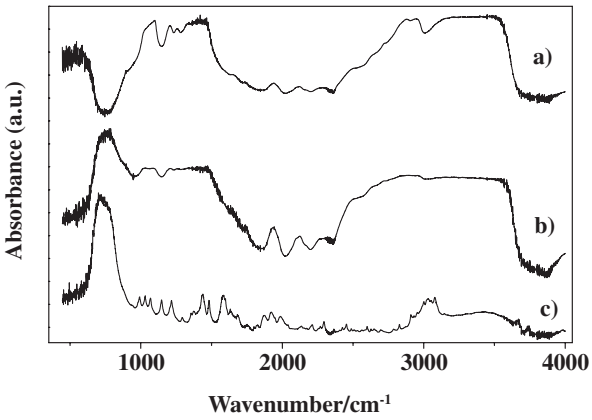

Figure 12. FT-IR spectra: a), b), and c) correspond to the pure ethylene glycol solution, the solution collected after extracting and pure pyridine solution, respectively.

solution were studied (Figure 12). Before (Figure 12a) and after extracting (Figure 12b), the FT-IR spectra of ethylene glycol solution did not change except the peak at about 750 cm^{-1} which should come from the pyridine. And the pyridine should come from the CuS/pyridine composite after extracting. This suggests that the redox reaction was not caused by the extraction solution of ethylene glycol. After extracting, the coordinate bonds between N (in pyridine) and Cu were destroyed. So the chemical properties became active around the surface of CuS crystalline regions and the redox reaction happened among CuS itself. The reaction function is shown as follows:

$$9CuS \xrightarrow[\text{under press}]{\Delta} Cu_9S_5 + 4S\downarrow \quad (1)$$

A little obtained S could dissolve in ethylene glycol and was removed with it. To determine whether a little resultant S can be dissolved in ethylene glycol during the reaction, a test experiment was also carried out. A quantity of sublimed sulfur was added to ethylene glycol for solvothermal reaction. The solvothermal conditions were the same as that of the extraction experiment. We found that the sublimed sulfur disappeared after the experiment and it must have dissolved in the ethylene glycol.

Why were pure Cu_9S_5 microspheres (sample **B**) and CuS/Cu_9S_5 composite microwires (sample **D**) obtained after the same extraction experiments? The reason is the different precursors (samples **A** and **C**) have different sub-nanostructures. According to the HR-TEM images (Figures 6a and 6c), we can see that the area of the crystalline zones of sample **A** (CuS/pyridine microspheres) were smaller than that of the crystalline bands of sample **C** (CuS/pyridine microwires). During the extraction experiments, it is reasonable to believe that the redox reaction happened in the entire crystalline zones of CuS in sample **A** but happened only on the surface of the crystalline bands of CuS in sample **C**. So after extraction, we obtained pure Cu_9S_5 microspheres from substrate **A** but CuS/Cu_9S_5 composite microwires from substrate **C** in which Cu_9S_5 grew around the surface of the CuS crystalline bands (Figures 6b and 6d).

Conclusion

Burr-like CuS/Cu_9S_5 microwires and Cu_9S_5 microspheres can be obtained by extracting the precursors of burr-like CuS/pyridine microwires and microspheres, respectively. The pyridine acted as both reactant and template in the first synthesis step. After extracting, the obtained CuS/Cu_9S_5 microwires (diameter of ca. 300 nm and length of several micrometers) and the Cu_9S_5 microspheres (diameter of ca. 800 nm) remained in the morphologies of their precursors largely. The XRD, FT-IR, and UV–vis absorption spectra indicated that the second solvothermal step can extract pyridine out of the composites completely. The same extracting process of CuS/pyridine microwires and microspheres but the different products of CuS/Cu_9S_5 microwires and Cu_9S_5 microspheres obtained here originated in the different internal structures of the different precursors, which can be see from their HR-TEM images. In a word, this two-step solvothermal synthesis is an effective method to obtain nanostructures with uniform morphologies and large products.

The authors gratefully thank the financial supports of Foundation and Front Technology Plan of He'nan Province (Grant No. 092300410165) and Nation Natural Science Foundation of China (Grant No. 10704073 and 50772042).

References

1 Q. Lu, F. Gao, D. Zhao, *Nano Lett.* **2002**, *2*, 725.
2 S. Gorai, D. Ganguli, S. Chaudhuri, *Cryst. Growth Des.* **2005**, *5*, 875.
3 Z.-D. Nan, C.-Z. Wei, X.-Y. Wang, H.-Y. Hao, *Chin. J. Chem.* **2008**, *26*, 1395.
4 H. Zhang, Y. Zhang, J. Yu, D. Yang, *J. Phys. Chem. C* **2008**, *112*, 13390.
5 Y. Huang, H. Xiao, S. Chen, C. Wang, *Ceram. Int.* **2009**, *35*, 905.
6 X. Jiang, Y. Xie, J. Lu, W. He, L. Zhu, Y. Qian, *J. Mater. Chem.* **2000**, *10*, 2193.
7 S. Lindroos, A. Arnold, M. Leskelä, *Appl. Surf. Sci.* **2000**, *158*, 75.
8 S. Erokhina, V. Erokhin, C. Nicolini, *Langmuir* **2003**, *19*, 766.
9 P. Roy, S. K. Srivastava, *Cryst. Growth Des.* **2006**, *6*, 1921.
10 X.-L. Yu, C.-B. Cao, H.-S. Zhu, Q.-S. Li, C.-L. Liu, Q.-H. Gong, *Adv. Funct. Mater.* **2007**, *17*, 1397.
11 W. Lou, M. Chen, X. Wang, W. Liu, *J. Phys. Chem. C* **2007**, *111*, 9658.
12 S. Li, H. Wang, W. Xu, H. Si, X. Tao, S. Lou, Z. Du, L. S. Li, *J. Colloid Interface Sci.* **2009**, *330*, 483.
13 G.-T. Zhou, X. Wang, J. C. Yu, *Cryst. Growth Des.* **2005**, *5*, 1761.
14 L. Fan, H. Song, H. Zhao, G. Pan, H. Yu, X. Bai, S. Li, Y. Lei, Q. Dai, R. Qin, T. Wang, B. Dong, Z. Zheng, X. Ren, *J. Phys. Chem. B* **2006**, *110*, 12948.
15 T. Sakamoto, H. Sunamura, H. Kawaura, T. Hasegawa, T. Nakayama, M. Aono, *Appl. Phys. Lett.* **2003**, *82*, 3032.
16 T. H. Larsen, M. Sigman, A. Ghezelbash, R. C. Doty, B. A. Korgel, *J. Am. Chem. Soc.* **2003**, *125*, 5638.
17 A.-M. Qin, Y.-P. Fang, H.-D. Ou, H.-Q. Liu, C.-Y. Su, *Cryst. Growth Des.* **2005**, *5*, 855.

18 R. Marshall, S. S. Mitra, *J. Appl. Phys.* **1965**, *36*, 3882.
19 P. Zhang, L. Gao, *J. Mater. Chem.* **2003**, *13*, 2007.
20 E. J. Silvester, F. Grieser, B. A. Sexton, T. W. Healy, *Langmuir* **1991**, *7*, 2917.
21 S. K. Haram, A. R. Mahadeshwar, S. G. Dixit, *J. Phys. Chem.* **1996**, *100*, 5868.
22 R. Córdova, H. Gómez, R. Schrebler, P. Cury, M. Orellana, P. Grez, D. Leinen, J. R. Ramos-Barrado, R. D. Río, *Langmuir* **2002**, *18*, 8647.
23 L. Reijnen, B. Meester, A. Goossens, J. Schoonman, *Chem. Mater.* **2005**, *17*, 4142.
24 A. A. Sagade, R. Sharma, *Sens. Actuators, B* **2008**, *133*, 135.